

Article

Robust Design Optimization with Penalty Function for Electric Oil Pumps with BLDC Motors

Keun-Young Yoon ¹ and Soo-Whang Baek ^{2,*}

¹ Department of Electrical Engineering, Honam University, 417 Eodeung-daero, Gwangsan-gu, Gwangju 62399, Korea; ky.yoon@honam.ac.kr

² Department of Automotive Engineering, Honam University, 417 Eodeung-daero, Gwangsan-gu, Gwangju 62399, Korea

* Correspondence: swbaek@honam.ac.kr; Tel.: +82-062-940-5408

Received: 29 November 2018; Accepted: 27 December 2018; Published: 2 January 2019

Abstract: In this paper, we propose and evaluate a robust design optimization (RDO) algorithm for the shape of a brushless DC (BLDC) motor used in an electric oil pump (EOP). The components of the EOP system and the control block diagram for driving the BLDC motor are described. Although the conventional deterministic design optimization (DDO) method derives an appropriate combination of design goals and target performance, DDO does not allow free searching of the entire design space because it is confined to preset experimental combinations of parameter levels. To solve this problem, we propose an efficient RDO method that improves the torque characteristics of BLDC motors by considering design variable uncertainties. The dimensions of the stator and the rotor were selected as the design variables for the optimal design and a penalty function was applied to address the disadvantages of the conventional Taguchi method. The optimal design results obtained through the proposed RDO algorithm were confirmed by finite element analysis, and the improvement in torque and output performance was confirmed through experimental dynamometer tests of a BLDC motor fabricated according to the optimization results.

Keywords: optimal design; oil pump; brushless DC; motor; robust; vehicles

1. Introduction

A hybrid vehicle combines two or more different power sources to obtain a driving force. In most cases, the power sources are an internal combustion engine that uses fuel and an electric motor driven by battery power. Hybrid vehicles drastically reduce fuel consumption and harmful gas emissions compared to conventional vehicles. In recent years, research on hybrid vehicles has been actively pursued in response to the demand for improved fuel efficiency and more environmentally friendly products [1–5].

The oil pump is an actuator between the engine and the electric motor and supplies the hydraulic fluid necessary for the transmission [6,7]. However, conventional oil pumps fail to deliver the required flow rate under operating conditions, thereby decreasing the vehicle's fuel efficiency [8]. To address this problem, an electric oil pump (EOP) has been developed that can supply a suitable flow rate under operating conditions [9,10]. Hybrid vehicles with conventional internal combustion engines use a mechanical oil pump to improve fuel economy and an EOP as an auxiliary; the EOP operates only when the mechanical oil pump stops, when the vehicle stops or travels at low speed, or when the transmission fluid flow is insufficient in the electric-vehicle mode. Thus, the EOP reduces mechanical power loss by operating only when the transmission requires oil pressure [11,12]. The EOP supplies the required flow rate to the engine clutch and the transmission by variably controlling the rotational speed of the EOP's drive motor according to the driving state of the vehicle and operator [13]. In addition to the oil pump installed inside the transmission, the hybrid vehicle also

has an external oil pump attached to the outside of the transmission to supply sufficient operating fluid to the engine clutch [14]. The EOP is controlled by a brushless DC (BLDC) motor in low- and high-speed modes in consideration of system efficiency and operation responsiveness according to the driving state of the vehicle and driver [15].

Recently, as competition in the international industrial market has become more intense, new design methods are required to satisfy increasingly stringent product performance and quality requirements [16]. In the conventional motor design process, deterministic design optimization (DDO) methods have been used to optimize design, assuming constant design variable values to maximize performance [17]. However, all motors exhibit inherent uncertainties in their material properties, manufacturing tolerances, and operating conditions. Conventional design techniques consider product uncertainties by implementing safety factors based on design experience [18]. However, these safety factors do not accurately quantify the limitations and uncertainties, and insufficient safety factor estimates can degrade motor performance and service life, whereas excessive safety factors increase production costs. Therefore, a robust design optimization (RDO) technique that can systematically consider stochastic uncertainties is required [19]. In RDO, unlike conventional design methods, design variables are defined as randomly distributed according to specific dispersion characteristics centered on mean values, and the relative probabilities are considered [20]. RDO approaches have double-loop optimization structures in which the probabilistic constraint added to the conventional optimal design process is optimized separately from the objective function. Therefore, RDO approaches, such as the Monte Carlo and worst-case simulations that have recently been applied to this problem, significantly increase the design time and computational costs, compared with the conventional optimal design method [21–23]. To address these problems, the Taguchi method has been proposed, whereby the main design factors influencing the product characteristics are selected and the optimal design combination is obtained with a minimum number of experiments. However, the Taguchi method the preset level values in the design space are limited to the available experimental combinations, and unrestricted searches of the entire design space are thus not permitted [24,25]. In addition, various constraints related to motor performance cannot be easily investigated in the given design time.

In this paper, with the objective of refining the Taguchi method to develop an evaluation technique that offers excellent convergence stability and calculation efficiency, we introduce an optimal level search method that incorporates the inequality constraint by adding a corresponding penalty function to the loss function. The optimal level search method guarantees the free movement of repeated design points in the design space by automatically adjusting the intervals of the set design parameter levels to identify successive experimental combinations. To verify feasibility, the proposed RDO method was applied to the design of a 150 W BLDC motor with an EOP, and the method's performance was compared with conventional DDO results obtained using finite element analysis. Finally, prototype BLDC motors were fabricated and dynamometer tests were performed to confirm the suitability of the proposed RDO in a practical application.

2. EOP System and BLDC Motor

2.1. EOP System

Conventional oil pumps are driven by the driving force of the engine, which causes power loss from the engine. As the number of engine revolutions increases, the oil flow rate increases more than necessary. Therefore, unnecessary power consumption occurs, and the engine output and fuel efficiency are reduced. To solve this problem, a (motor-driven) EOP that is mechanically independent of the engine speed has been developed. EOPs provide the fluid pressure and flow rate required for the transmission and are especially useful in vehicles equipped with the "Idle Stop & Go" system function, where the EOPs reduce the shift shock that can occur with the automatic transmission because of lack of flow after stopping or starting the vehicle, thereby improving fuel economy and reducing exhaust gas. The EOP system consists of a motor, a motor driver, and a pump assembly for generating hydraulic fluid, as shown in Figure 1. The motor is a three-phase BLDC motor with a Hall

sensor, and the motor driver uses a three-phase full bridge circuit consisting of an N-channel metal-oxide field-effect transistor (MOSFET). The motor driver controls the hydraulic pressure of the transmission to maintain suitable low-speed, reverse, or stop conditions.

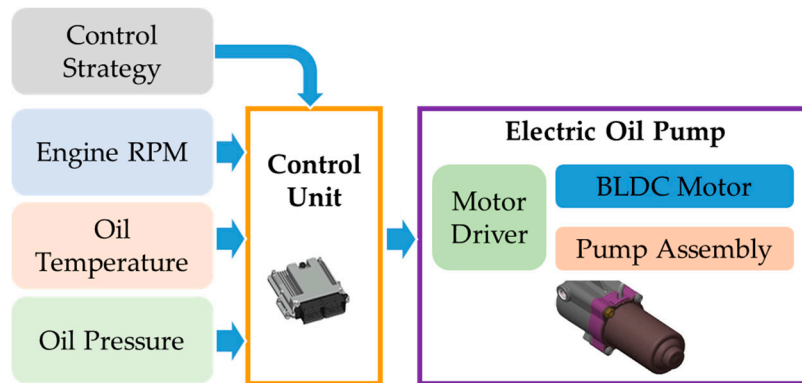


Figure 1. Configuration of the electric oil pump (EOP) system.

Figure 2 is a block diagram of the EOP’s control unit, which includes a power supply unit that receives the vehicle battery power and supplies the required voltage to each device; a microcontroller unit (MCU) that receives the target rotational speed (rpm) of the EOP motor and outputs a pulse width modulation (PWM) control signal to the motor driver; a motor control unit; and a motor driving unit that supplies current to the motor by switching MOSFETs. The motor driving unit consists of six MOSFET switches that are sequentially turned on and off according to the signal provided by the motor control unit, which includes logic for turning the six MOSFETs on and off, as well as a Hall sensor input for detecting the position of the rotor, a function for diagnosing disconnection and short circuit of the motor, and a gate drive circuit for turning the MOSFETs on and off.

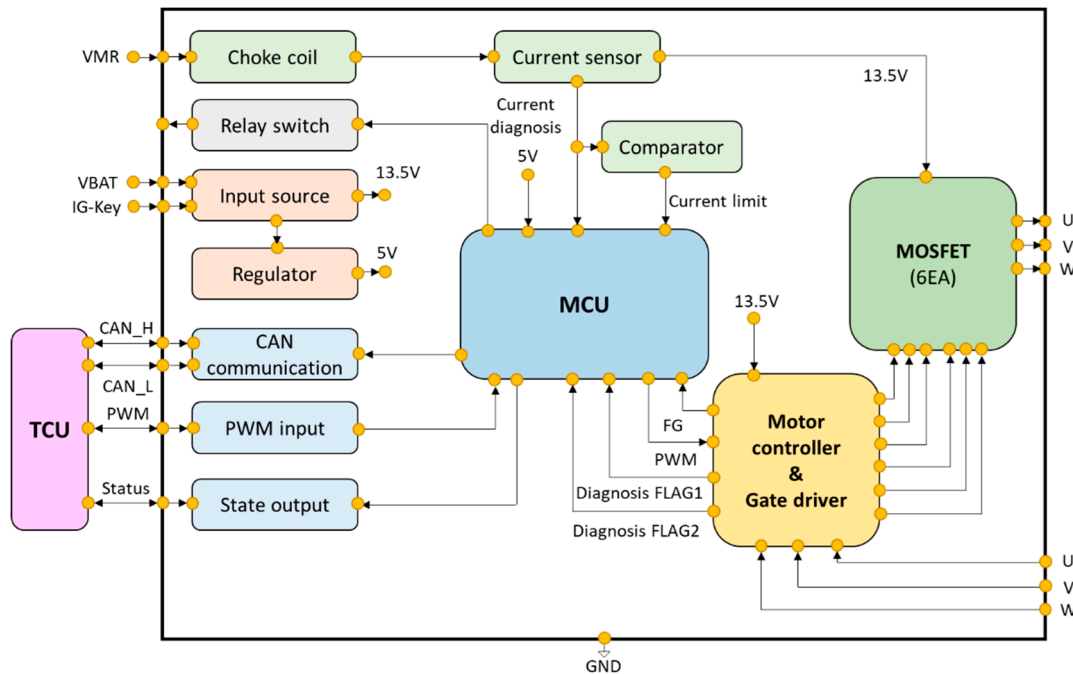


Figure 2. Block diagram of the EOP control unit.

The power supply uses three sources, as shown in Figure 2. The constant power source (VBAT) is supplied from the vehicle battery. The isolated ground (IG) power (IG-Key) is supplied only when the vehicle is started. The relay power supply (VMR) is entirely dedicated to the motor driver FET. The power unit receives the constant power supply and outputs 13.5 V and 5 V to the motor control unit and to the MCU and Hall sensor of the BLDC motor, respectively. When the IG power is turned

on with constant power available, the MCU operates for a certain period of time using the constant power even after the IG power is turned off. The MCU is a key component for driving the oil pump and manages all operating procedures. When IG power is on, the MCU operates and controller area network communication is activated; the MCU diagnoses the internal condition and informs the transmission control unit of the abnormality via controller area network communication. When the transmission control unit receives an instruction to drive the motor, the transmission control unit turns on the external relay to supply power via the VMR and drive the motor. In addition, a PWM waveform is supplied to the motor control section to control the speed of the BLDC motor. The current value flowing through the motor is sensed by the current sensor, and the maximum current value is limited during overcurrent. To protect the system, when the maximum current continues to flow for a certain period of time, the MCU enters the power save mode and limits the current value to a lower level. The set BLDC motor speed is provided continuously from the transmission control unit to the MCU via controller area network communication or the PWM value, which acts as a backup for when the controller area network communication is disconnected. The MCU also provides the internal control status of the EOP control unit to the transmission control unit as a status update in preparation for controller area network disconnection.

2.2. BLDC Motor

Figure 3 shows the shape of a conventional BLDC motor used for an EOP, the specifications of which are presented in Table 1.

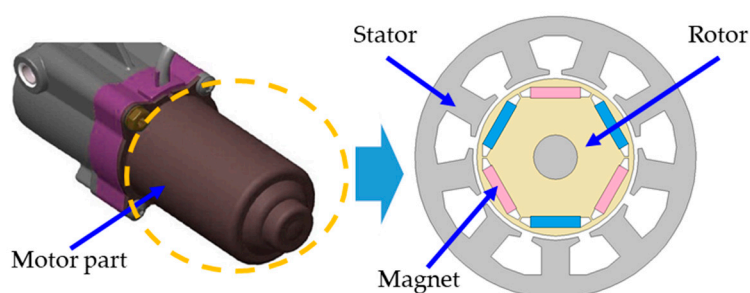


Figure 3. Shape of conventional brushless DC (BLDC) motor for an EOP.

Table 1. Specifications of the conventional BLDC motor.

	Items	Value	Unit
Stator	Outer/Inner diameter	51/30	mm
	Slots	9	-
	Number of turns	14	turns
Rotor	Outer/Inner diameter	29/8	mm
	Pole	6	-
	Magnet grade	N42EH	NdFeB
Rated	Speed	4000	rpm
	Output power	150	W
	Efficiency	70	%
	Torque	0.358	Nm
	Stack length	35	mm
	Air-gap length	0.5	mm
	Maximum speed	6000	rpm
	Cogging torque (peak to peak)	0.037	Nm
	Torque ripple (peak to peak)	0.06	Nm

The conventional BLDC motor selected for this study had a six-pole nine-slot structure, of the concentrated-winding interior permanent magnet (IPM) type, considering vibration and noise. An

initial design was established to satisfy the given specifications. The current density of the stator windings was designed to be less than $6 \text{ A}_{rms}/\text{mm}^2$ at maximum speed. In this study, a previously reported torque per unit rotor volume (TRV) was used to establish the dimensions of the rotor [26]. The rotor diameter can be estimated using maximum torque, TRV, and stack length (rotor and stator axial length) and can be expressed as

$$D_r = \sqrt{\frac{4 \cdot T}{TRV \cdot \pi \cdot L_{stack}}} \quad (1)$$

where D_r is the diameter of the rotor, T is the maximum torque of the BLDC motor and L_{stack} is the stack length.

3. Methods

3.1. RDO Process

Figure 4 summarizes the RDO concept. If there is a design variable that varies with any distribution of the other system design variables, the response of the system to the first design variable should also appear as a distribution rather than as a single value. In such cases, RDO is executed to narrow the variation range of the objective function with respect to the variation of the design variables, applying constraints to ensure that the optimal design point is feasible.

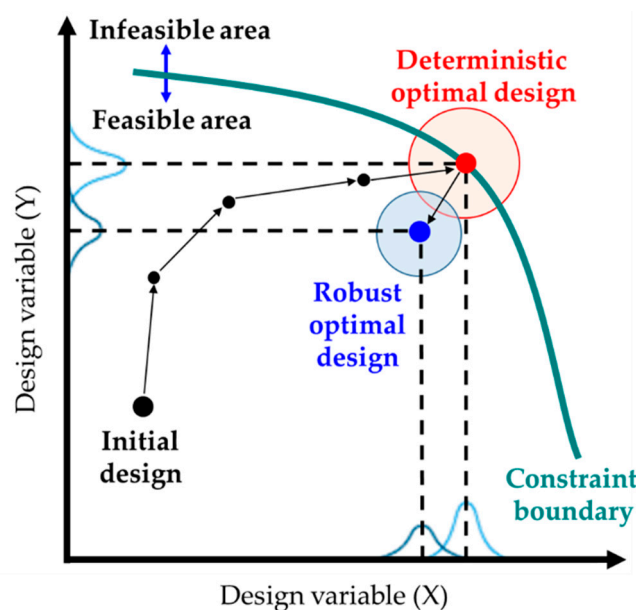


Figure 4. Robust design optimization (RDO) concept.

RDO thus minimizes a specific objective function at a set constraint. In this paper, the Taguchi method is modified as follows to enhance efficiency. In the Taguchi method, the loss that occurs as the product performance moves away from the target value is expressed as a loss function, defined based on the signal-to-noise ratio (SNR) to target a specific value, a maximum value, or a minimum value [27,28]. In this study, we use the loss function shown in Equation (2), which targets a minimum but non-negative value.

$$SNR = -\log \left[\frac{1}{n} \sum_{i=1}^n y_i^2 \right] \quad (2)$$

Here, y_i is the performance value of the performance function h derived from the i th experimental combination, and n is the total number of experimental combinations.

The conventional Taguchi method derives the optimal combination of experiments using the SNR only for the specific target performance of the design object. However, a general RDO must

consider multiple targets simultaneously, as well as other performance-related constraints, and we therefore introduce a penalty function that is added to the performance value y_i for the performance function h , as in Equation (3), to account for the constraints. That is, the penalty function increases in value according to the degree of violation of the constraint condition.

$$\hat{y}_i = h(X) + W_p P(X) \quad (3)$$

Here, the performance value derived from the re-defined experimental combination includes the penalty function: W_p is the weight of the penalty function, and $P(X)$ is the penalty function considering the constraint. The definition of the penalty function used in this paper is expressed as Equation (4).

$$P(X) = \sum_{j=1}^{np} [\text{maximum}\{0, C(X)\}^2] \quad (4)$$

where C is a constraint. If all constraints are satisfied, the penalty function value becomes zero. However, if the constraint condition is violated, the square of the constraint condition value is applied to the penalty function.

To find the optimal solution by continuously searching the designated design space using the Taguchi method, the level of each design factor used to construct each experimental combination should be automatically changed. That is, when the design point moves in response to the optimal combination result derived from the current experimental combination, a new combination of experiments is constructed at the new design point. At this time, if a new level value is determined for each design factor, a more advanced design point search is possible. In this study, three design factor levels were defined: the interval between levels 1 and 2, Δ_1 , and the interval between levels 2 and 3, Δ_2 . The values of the current levels 1, 2, and 3 were set as X_{1prev} , X_{2prev} , and X_{3prev} , respectively. The new level values (X_1 , X_2 , X_3) for the subsequent experiment combination were then defined as shown in Table 2 according to the optimal level value derived from the current experimental combination.

Table 2. Definition of new level values.

Items	Description
Case #1 When X_1 is determined as the optimal level	$X_1 = X_{1prev} - \Delta_1$
	$X_2 = X_{1prev}$
	$X_3 = X_{2prev}$
Case #2 When X_2 is determined as the optimal level	$X_1 = X_{2prev} - \Delta_1/2$
	$X_2 = X_{2prev}$
	$X_3 = X_{2prev} + \Delta_2/2$
Case #3 When X_3 is determined as the optimal level	$X_1 = X_{2prev}$
	$X_2 = X_{3prev}$
	$X_3 = X_{2prev} + \Delta_2$

Figure 5 shows the proposed RDO algorithm with the penalty function and the optimal level search method.

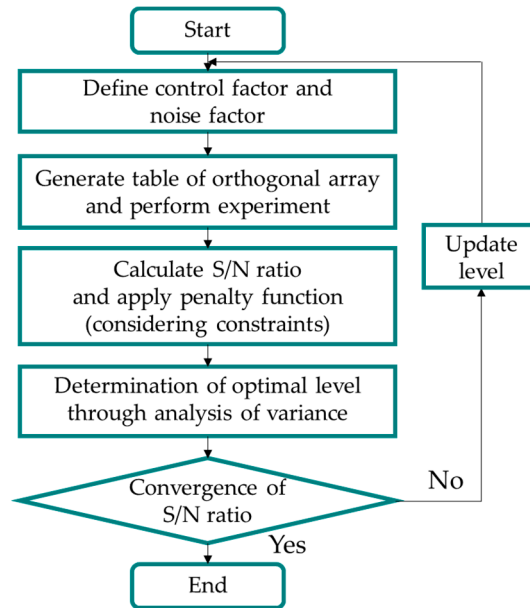


Figure 5. Proposed RDO algorithm.

The iterative design process of the proposed Taguchi method modification is as follows.

- (1) Define noise factors caused by control factors and design variable uncertainties.
- (2) Configure experimental combinations according to an orthogonal array table and perform experiments.
- (3) Calculate the SNR to which the penalty function is added considering the constraint condition.
- (4) Determine the optimal experimental combination based on the design factor levels estimated through analysis of variance.
- (5) If the SNR does not converge to the set value, repeat steps (2) through (4) using the new levels identified in the optimal level search.
- (6) When the SNR converges to the set value, the design process is complete.

To verify the feasibility of the proposed RDO, the method was applied to the BLDC motor described in Table 1, which drives an EOP with a rated output of 150 W, rated torque of 0.358 Nm, and rated speed of 4000 rpm. In BLDC motors, cogging torque is generated by a permanent magnet, flux barrier, and stator slot structure, which causes vibration and noise. Therefore, in this study, to minimize the cogging torque of the conceptually designed motor, five major design variables were set as shown in Figure 6.

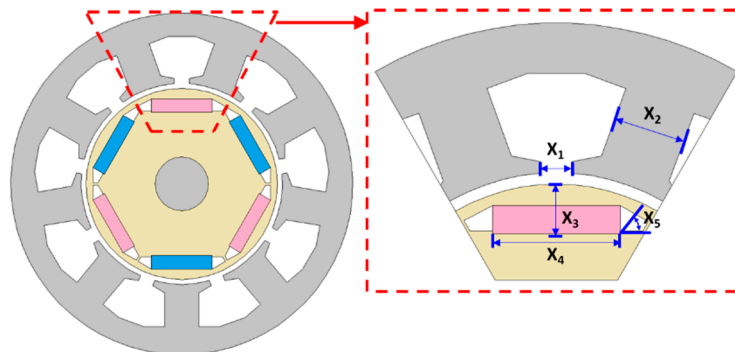


Figure 6. Cross-section of the BLDC motor and design variables. where X_1 is the length of slot opening, X_2 is the width of stator tooth, X_3 is the position of permanent magnet from rotor outer diameter, X_4 is the length of permanent magnet and X_5 is the angle between permanent magnet and magnetic flux barrier.

ANSYS Electromagnetics Suite 18.0, a commercial electromagnetic analysis tool based on finite element analysis, was used to simulate the experimental combinations of the Taguchi method. For comparison, the conventional DDO and the proposed RDO techniques were each applied to the motor cogging torque reduction design.

3.2. DDO Process

The maximum cogging torque of the BLDC motor to be designed is defined as an objective function f . In this case, the objective function, given by Equation (5), is minimized by considering the following two performance constraints: C_1 , whereby the rated torque of an optimized motor shall be greater than 0.358 Nm, and C_2 , whereby the cogging torque of the optimized motor should be less than 24.85% of the torque ripple of the conventional motor.

$$\begin{aligned} & \text{Minimize } f(X) \\ & \text{Subject to } C_1(X) = 0.358 - T_{rated} \leq 0, \quad C_2(X) = \frac{T_{max} - T_{min}}{T_{rated}} \times 100 - 24.85 \leq 0 \\ & X_L \leq X \leq X_U \end{aligned} \quad (5)$$

Here, T_{rated} is the rated torque; T_{max} and T_{min} are the maximum and minimum torque ripple, respectively; X_L and X_U are the set lower and upper limits of each design variable, the values of which are shown in Table 3. The optimal solution of the design problem given by Equation (5), excluding the fluctuation of design variables due to uncertainty, was explored by applying sequential quadratic programming.

Table 3. Design and noise factors of the BLDC motor.

Items	Parameters	Level 1	Level 2	Level 3	Unit	X_L	X_U
						Lower	Upper
Design factor	X_1	2.1	2.2	2.3	mm	1.5	2.5
	X_2	5.0	5.1	5.2	mm	4.5	5.5
	X_3	3.44	3.54	3.64	mm	3.0	4.0
	X_4	8.9	9.0	9.1	mm	8.0	10.0
	X_5	18.9	19.0	19.1	degree	10	60
Noise factor	-	Level 1	Level 1	Level 1	-	-	-
Tolerance	-	-0.1	0	0.1	-	-	-

3.3. RDO Definition

To formulate the RDO problem using the proposed method, the penalty function $P(X)$ was constructed using the average torque C_1 and the torque ripple C_2 , which were the Equation (5) constraints, and a new performance value was defined, as shown in Equation (6).

$$\begin{aligned} & \text{Minimize } T_{cog} : f = -10 \log \left[\frac{1}{n} \sum_{i=1}^n y_i'^2 \right] \\ & y_i' = h(X) + W_p P(X) \\ & P(X) = \sum_{j=1}^{np} \left[\text{maximum}\{0, C_j(X)\}^2 \right] \end{aligned} \quad (6)$$

Here, T_{cog} is the cogging torque, and the value of the weight W_p of the penalty function is set to 1.

When an experimental combination violated a constraint, the penalty function increased the performance value such that it was excluded from the optimal combination selection. All design factors were assigned three levels, and experimental combinations were constructed using an L18(3⁵) orthogonal array of five factors with three levels each, without considering alternation. The variation

of the objective function caused by a tolerance of ± 0.1 was calculated through analysis of variance by setting the uncertainty caused by the manufacturing tolerance of a design factor as a noise factor.

4. Verification

4.1. Simulation Results

Figure 7 compares the shapes derived from the DDO and the proposed RDO methods, based on the design parameter values of the conventional model. The optimal design models provided by both methods had the same stator and rotor dimensions, winding specifications and permanent magnet amounts as the conventional model.

Figure 8 shows the characteristics of the cogging torque. One cycle of the cogging torque had a mechanical angle of 20 degrees per motor revolution, based on the least common multiple of 18 of the nine slots and six poles. The cogging torque characteristics represent the difference between the maximum and minimum values, which were 0.037, 0.019, and 0.011 Nm according to the conventional, DDO, and proposed RDO models, respectively. These results confirmed analytically that the value of cogging torque decreases with optimization, which was attributed to the reduced magnetic reluctance in the air gap between the BLDC's stator and rotor due to their optimized shapes.

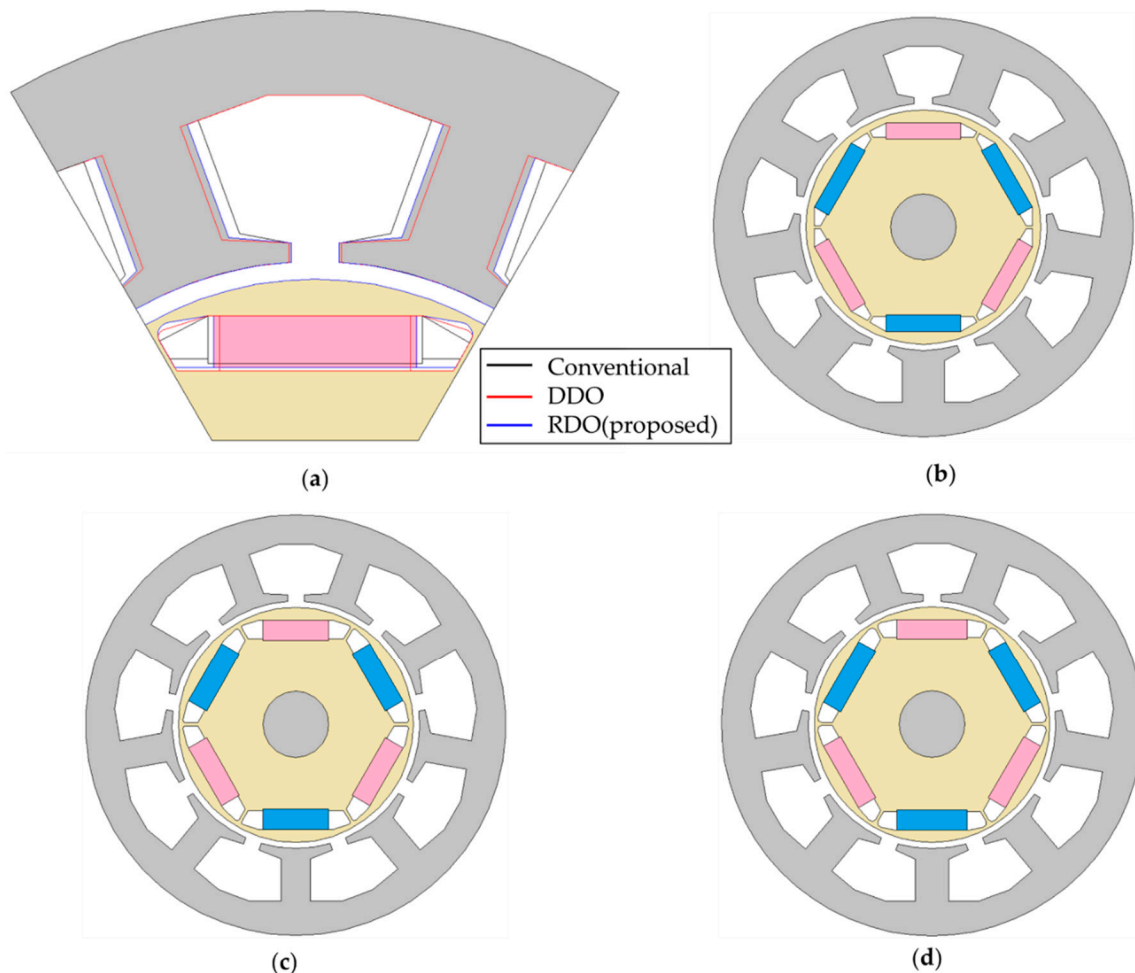


Figure 7. Shape comparison: (a) Comparison; (b) Conventional; (c) Deterministic design optimization (DDO); (d) RDO (proposed).

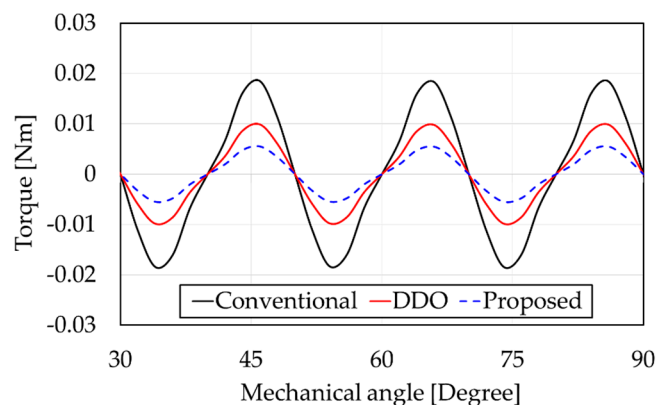


Figure 8. Cogging torque characteristic comparison.

Figure 9 compares the characteristics of the torque ripple, which was 0.087, 0.052, and 0.017 Nm according to the conventional, DDO, and proposed RDO models, respectively. These results confirmed that the proposed RDO method reduces the torque ripple characteristic compared to the conventional and DDO models.

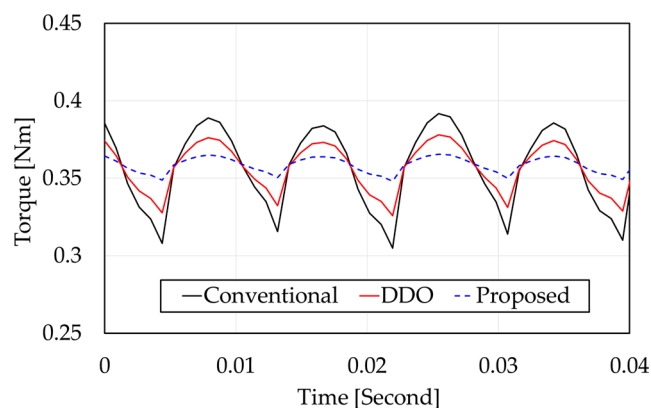


Figure 9. Torque ripple characteristic comparison.

Table 4 compares the design values derived from the DDO and proposed RDO methods, based on the design parameter values of the conventional model. When tolerances of ± 0.1 were included in the design parameters, the cogging torque (T_{cog}), torque ripple (T_{ripple}), and standard deviation of the maximum cogging torque (σ_{cog}) appeared in each of the three motor designs. Both the DDO and proposed RDO results satisfied the constraints on rated torque and torque ripple. Table 4 also shows the number of iterations and simulations that the DDO and proposed RDO methods required to derive the optimal design values for the BLDC motor.

Table 4. Design values and characteristics.

Items	Conventional	DDO	RDO	Unit
X_1	2.2	2.2	2.0	mm
X_2	5.1	3.5	4.1	mm
X_3	3.54	3.84	3.7	mm
X_4	9.0	8.0	8.5	mm
X_5	19.0	33.0	42.0	degree
T_{cog}	0.037	0.019	0.011	Nm
T_{ripple}	0.087	0.052	0.017	Nm
σ_{cog}	-	0.0484	0.0315	-
Iterative designs	-	9	15	-
Required simulations	-	124	336	-

4.2. Experimental Results

To verify the proposed RDO method, a prototype of the optimal BLDC motor was fabricated. The prototype BLDC motor assembly, stator, and rotor are shown in Figure 10. The stator had a split core structure to increase the winding fill factor in the slot. The rotor used NdFeB magnets rated at N42EH with high output density and excellent high-temperature demagnetization characteristics, in consideration of the environment in which the EOP would be mounted on the vehicle.

To measure the performance of the BLDC motors thus designed, a motor dynamometer test environment was constructed as shown in Figure 11.

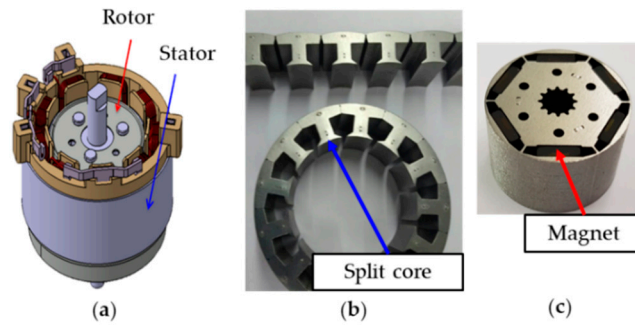


Figure 10. Prototype of optimal design: (a) Assembly; (b) Stator; (c) Rotor.

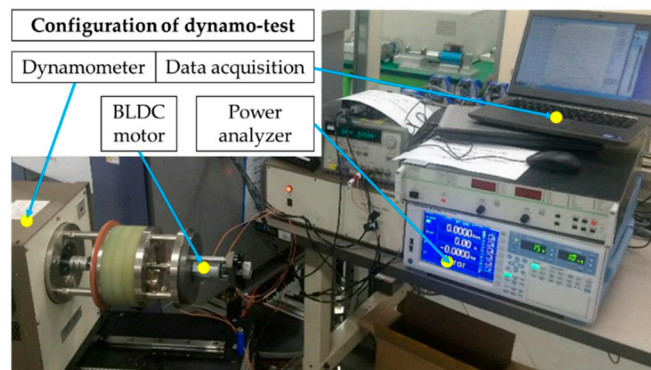


Figure 11. Experimental setup.

Figure 12 shows the experimentally determined cogging torque characteristics. The experimental results showed that the cogging torque characteristics were 0.071, 0.046, and 0.014 Nm for the conventional, DDO, and proposed RDO models, respectively. The experimental characteristics of the cogging torque were consistent with the decreasing tendency of the analytical results, despite some value differences due to the inertia of the test apparatus. In particular, the characteristics of the model identified by the proposed RDO method were clearly the most reduced.

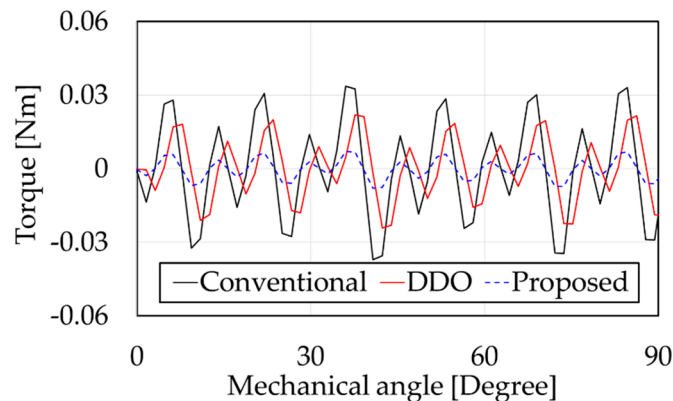


Figure 12. Comparison of experimentally determined cogging torque characteristics.

The BLDC motor performance was tested using the conventional, DDO, and proposed RDO models, and the results are shown in Figure 13.

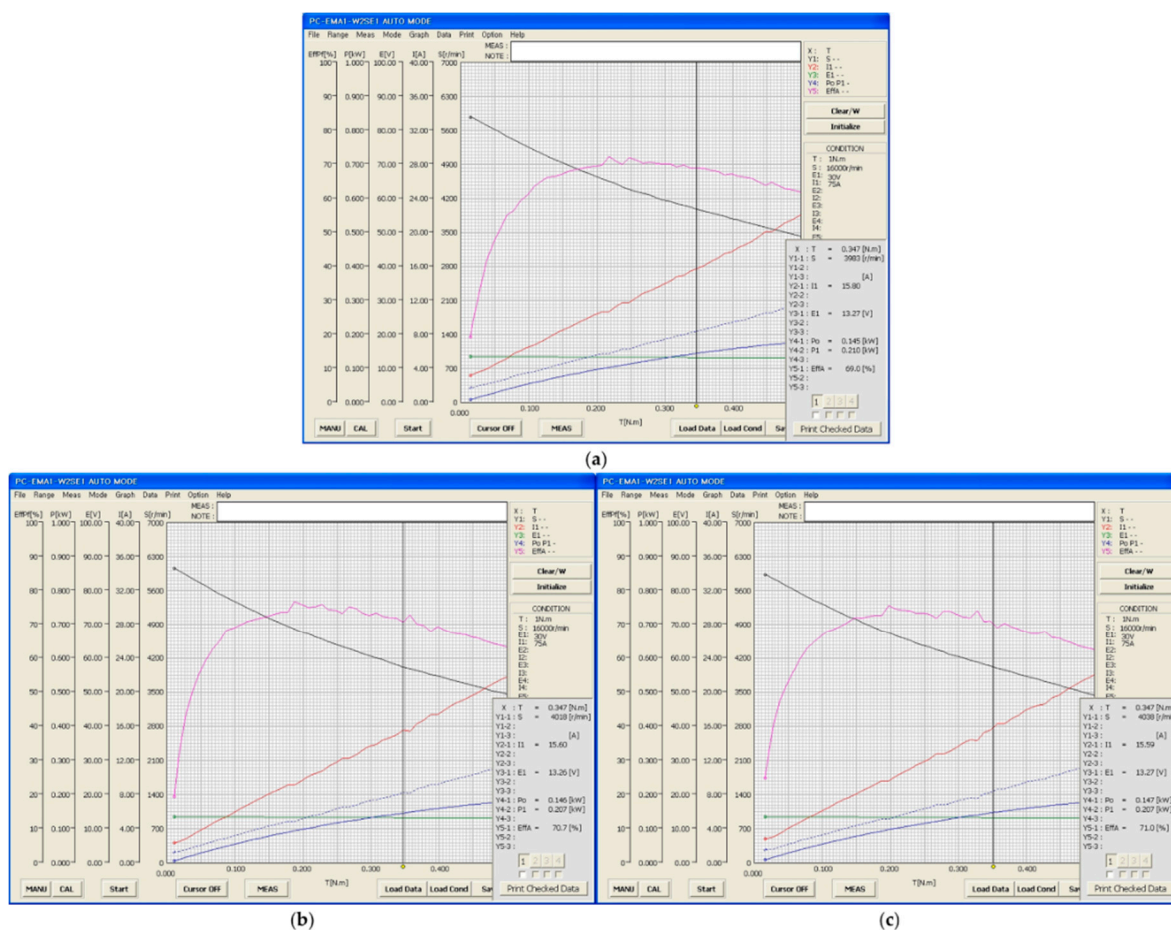


Figure 13. Comparison of experimental motor dynamometer test results: (a) Conventional; (b) DDO; (c) Proposed.

The measurement targets were speed and rated efficiency in response to increased load. The input voltage was 13.5 V DC. To compare the operating characteristics, the BLDC motor was started at a no-load speed of 6000 rpm and the load torque was continuously increased during the experiment. The experimental results showed that the rated efficiency of the conventional model was 69.0%, that of the DDO model was 70.7%, and that of the RDO model was 71.0%, under the rated operating conditions (rotational speed of 4000 rpm and output of 150 W). The rated efficiency of the test results of the conventional model was reduced by approximately 1.0% compared to the analysis results because the long lead wire used in the experiment increased the terminal resistance, and the magnitude of the resistance can have a large effect on the terminal voltage. The voltage dropped as the terminal resistance increased, and the copper loss was increased, resulting in a difference in voltage and efficiency characteristics. These results show that the rated efficiency of the proposed RDO model exceeds that of the conventional and DDO models. Table 5 summarizes the simulation and experimental results from each model.

Table 5. Simulation and experimental results.

	Items	Conventional	DDO	RDO	Unit
Simulation	Cogging torque	0.037	0.019	0.011	Nm
	Torque ripple	0.087	0.052	0.017	Nm
	Rated efficiency	70.0	71.2	72.2	%
Experiment	Cogging torque	0.071	0.046	0.014	Nm

Torque ripple	0.155	0.097	0.055	Nm
Rated efficiency	69.0	70.7	71.0	%

5. Conclusions

In this paper, we optimized the torque characteristics of a BLDC motor used in an EOP system. The design domain was set to have a normal distribution, and an orthogonal array table was applied to minimize the analysis in the design domain. To address inequality constraints, Taguchi proposed a penalty function method for the limited optimization problem, whereby the optimal level is determined from experimental results and parameter levels are changed accordingly. In this study, this constraint was applied to the design method by adding a penalty function associated with the constraint to the loss function and adjusting the parameter level intervals by applying an optimal level search method. Based on the performance of existing BLDC motors used in EOPs, we compared the DDO and RDO results by performing finite element analysis and experimental dynamometer testing. With the proposed RDO method, the cogging torque is reduced to 19%, the fluctuation of torque ripple is reduced to 35%, and the rated efficiency characteristic is improved by 2% compared with the conventional model. The proposed RDO improved the Taguchi method and was shown to be robust in comparison with DDO, although the number of iterations required was large. The cumulative results confirm that the proposed RDO algorithm improves the cogging torque, torque ripple, and rating efficiency characteristics of BLDC motors and is expected to improve the flow control stability when implemented in an EOP system in a test vehicle in the future.

Author Contributions: Conceptualization, S.-W.B.; Methodology, K.-Y.Y. and S.-W.B.; Software, K.-Y.Y. and S.-W.B.; Validation, K.-Y.Y. and S.-W.B.; Writing—original draft preparation, K.-Y.Y.; Writing—review and editing, S.-W.B.; Supervision, S.-W.B.; Funding acquisition, S.-W.B.

Acknowledgments: This study was supported by the National Research Foundation of Korea (NRF) grant funded by the Korea government (MSIT) (No. 2017R1C1B5075525); this study was also supported by a 2018 research fund from Honam University.

Conflicts of Interest: The authors declare no conflict of interest.

References

1. He, H.; Liu, Z.; Zhu, L.; Liu, X. Dynamic Coordinated Shifting Control of Automated Mechanical Transmissions without a Clutch in a Plug-In Hybrid Electric Vehicle. *Energies* **2012**, *5*, 3094–3109.
2. Chen, J.-S. Energy Efficiency Comparison between Hydraulic Hybrid and Hybrid Electric Vehicles. *Energies* **2015**, *8*, 4697–4723.
3. Chen, Z.; Xiong, R.; Wang, K.; Jiao, B. Optimal Energy Management Strategy of a Plug-in Hybrid Electric Vehicle Based on a Particle Swarm Optimization Algorithm. *Energies* **2015**, *8*, 3661–3678.
4. Xia, C.; DU, Z.; Zhang, C. A Single-Degree-of-Freedom Energy Optimization Strategy for Power-Split Hybrid Electric Vehicles. *Energies* **2017**, *10*, 896.
5. Capata, R. Urban and Extra-Urban Hybrid Vehicles: A Technological Review. *Energies* **2018**, *11*, 2924.
6. Doikin, A.; Habib Zadeh, E.; Campean, F.; Priest, M.; Brown, A.; Sherratt, A. Impact of Duty Cycle on Wear Progression in Variable-displacement Vane Oil Pumps. *Procedia Manuf.* **2018**, *16*, 115–122, doi:10.1016/j.promfg.2018.10.170.
7. Rostek, E.; Babiak, M.; Wróblewski, E. The Influence of Oil Pressure in the Engine Lubrication System on Friction Losses. *Procedia Eng.* **2017**, *192*, 771–776, doi:10.1016/j.proeng.2017.06.133.
8. Podevin, P.; Clenci, A.; Decombes, G. Influence of the lubricating oil pressure and temperature on the performance at low speeds of a centrifugal compressor for an automotive engine. *Appl. Therm. Eng.* **2011**, *31*, 194–201, doi:10.1016/j.applthermaleng.2010.08.033.
9. Miyachi, E.; Ishiguro, M.; Mizumoto, K. *Development of Electric Oil Pump*; SAE Technical Paper; SAE International: Warrendale, PA, USA, 2006; 2006-01-1595, doi:10.4271/2006-01-1595.
10. Kim, Y.; Lee, J.; Jo, C.; Kim, Y.; Song, M.; Kim, J.; Kim, H. Development and Control of an Electric Oil Pump for Automatic Transmission-Based Hybrid Electric Vehicle. *IEEE Trans. Veh. Technol.* **2011**, *60*, 1981–1990, doi:10.1109/TVT.2011.2140135.

11. Kim, H.; Wi, J.; Yoo, J.; Son, H.; Park, C.; Kim, H. A Study on the Fuel Economy Potential of Parallel and Power Split Type Hybrid Electric Vehicles. *Energies* **2018**, *11*, 2103.
12. Zhang, X.; Li, C.-T.; Kum, D.; Peng, H. Prius+ and Volt-: Configuration Analysis of Power-Split Hybrid Vehicles with a Single Planetary Gear. *IEEE Trans. Veh. Technol.* **2012**, *61*, 3544–3552.
13. Zhao, Z.; He, L.; Yang, Y.; Wu, C.; Li, X.; Karl Hedrick, J. Estimation of torque transmitted by clutch during shifting process for dry dual clutch transmission. *Mech. Syst. Signal Process.* **2016**, *75*, 413–433, doi:10.1016/j.ymssp.2015.12.027.
14. Della Gatta, A.; Iannelli, L.; Pisaturo, M.; Senatore, A.; Vasca, F. A survey on modeling and engagement control for automotive dry clutch. *Mechatronics* **2018**, *55*, 63–75, doi:10.1016/j.mechatronics.2018.08.002.
15. Song, M.; Oh, J.; Kim, J.; Kim, Y.; Yi, J.; Kim, Y.; Kim, H. Development of an electric oil pump control algorithm for an automatic-transmission-based hybrid electric vehicle considering the gear shift characteristics. *Proc. Inst. Mech. Eng. Part D J. Automob. Eng.* **2013**, *228*, 21–36, doi:10.1177/0954407013497898.
16. Tu, J.; Choi, K.; Park, Y.H. A New Study on Reliability-Based Design Optimization. *J. Mech. Des.* **1999**, *121*, 557–564, doi:10.1115/1.2829499.
17. Kim, N.; Kim, D.; Kim, D.; Kim, H.; Lowther, D.; Sykulski, J. Robust Optimization Utilizing the Second-Order Design Sensitivity Information. *IEEE Trans. Magn.* **2010**, *46*, 3117–3120, doi:10.1109/TMAG.2010.2043719.
18. Lagaros, N.D.; Papadrakakis, M. Robust seismic design optimization of steel structures. *Struct. Multidisc. Optim.* **2007**, *33*, 457–469, doi:10.1007/s00158-006-0047-5.
19. Liu, C.; Lei, G.; Ma, B.; Guo, Y.; Zhu, J. Robust Design of a Low-Cost Permanent Magnet Motor with Soft Magnetic Composite Cores Considering the Manufacturing Process and Tolerances. *Energies* **2018**, *11*, 2025.
20. Jun, C.-S.; Kwon, B.-I.; Kwon, O. Tolerance Sensitivity Analysis and Robust Optimal Design Method of a Surface-Mounted Permanent Magnet Motor by Using a Hybrid Response Surface Method Considering Manufacturing Tolerances. *Energies* **2018**, *11*, 1159.
21. Zhan, S.; Li, Z.; Hu, J.; Liang, Y.; Zhang, G. Model Order Identification for Cable Force Estimation Using a Markov Chain Monte Carlo-Based Bayesian Approach. *Sensors* **2018**, *18*, 4187.
22. Sun, Y.; Zhu, F.; Chen, J.; Li, J. Risk Analysis for Reservoir Real-Time Optimal Operation Using the Scenario Tree-Based Stochastic Optimization Method. *Water* **2018**, *10*, 606.
23. Choi, S.-H.; Hussain, A.; Kim, H.-M. Adaptive Robust Optimization-Based Optimal Operation of Microgrids Considering Uncertainties in Arrival and Departure Times of Electric Vehicles. *Energies* **2018**, *11*, 2646.
24. Pervez, M.N.; Shafiq, F.; Sarwar, Z.; Jilani, M.M.; Cai, Y. Multi-Response Optimization of Resin Finishing by Using a Taguchi-Based Grey Relational Analysis. *Materials* **2018**, *11*, 426.
25. Hong, G.; Wei, T.; Ding, X.; Duan, C. Multi-Objective Optimal Design of Electro-Hydrostatic Actuator Driving Motors for Low Temperature Rise and High Power Weight Ratio. *Energies* **2018**, *11*, 1173.
26. Hendershot, J.R.; Miller, T.J.E. *Design of Brushless Permanent-Magnet Machines*, 2nd ed.; Motor Design Books LLC: Venice, FL, USA, 2010.
27. Tseng, K.-H.; Shiao, Y.-F.; Chang, R.-F.; Yeh, Y.-T. Optimization of Microwave-Based Heating of Cellulosic Biomass Using Taguchi Method. *Materials* **2013**, *6*, 3404–3419.
28. Solehati, N.; Bae, J.; Sasmito, A.P. Optimization of Wavy-Channel Micromixer Geometry Using Taguchi Method. *Micromachines* **2018**, *9*, 70.

